

POWER SPECTRUM OF THE DENSITY OF COLD ATOMIC GAS IN THE GALAXY TOWARD CASSIOPEIA A AND CYGNUS A

A. A. DESHPANDE AND K. S. DWARAKANATH
Raman Research Institute, Bangalore 560 080, India

AND

W. M. GOSS
National Radio Astronomy Observatory, P.O. Box O, Socorro, NM 87801
Received 2000 May 16; accepted 2000 June 5

ABSTRACT

We have obtained the power spectral description of the density and opacity fluctuations of the cold H I gas in the Galaxy toward Cas A and Cygnus A. We have employed a method of deconvolution, based on CLEAN, to estimate the true power spectrum of optical depth of cold H I gas from the observed distribution, taking into account the finite extent of the background source and the incomplete sampling of optical depth over the extent of the source. We investigate the nature of the underlying spectrum of density fluctuations in the cold H I gas which would be consistent with that of the observed H I optical depth fluctuations. These power spectra for the Perseus arm toward Cas A and for the outer arm toward Cygnus A have a slope of 2.75 ± 0.25 (3σ error). The slope in the case of the Local arm toward Cygnus A is 2.5 and is significantly shallower in comparison. The linear scales probed here range from 0.01 to 3 pc. We discuss the implications of our results, the non-Kolmogorov nature of the spectrum, and the observed H I opacity variations on small transverse scales.

Subject headings: ISM: structure — methods: data analysis — radio lines: ISM — techniques: image processing — techniques: interferometric — turbulence

1. INTRODUCTION

The cold atomic gas in the Galaxy has been observed for over 40 years in the 21 cm H I line. These early single-dish and interferometric observations established the presence of cold atomic gas in the Galaxy, possibly in the form of discrete “clouds” in pressure equilibrium with the warm neutral medium (Clark, Radhakrishnan, & Wilson 1962; Clark 1965; Radhakrishnan et al. 1972; Field, Goldsmith, & Habing 1969; Field 1973). These H I clouds, with an estimated mean spin temperature of ~ 80 K and a mean density of $\sim 30 \text{ cm}^{-3}$, were thought to be a few parsecs in size. This simple picture of the cold gas has changed significantly during the last two decades due to high-resolution 21 cm line absorption measurements of the Galaxy made using aperture synthesis telescopes (Greisen 1973; Lockhart & Goss 1978; Bregman et al. 1983; Schwarz et al. 1986, 1995). Fine structures in the atomic hydrogen gas have been observed over a wide range, in length scales down to about 0.1 pc (Crovisier, Dickey, & Kazes 1985; Kalberla, Schwarz, & Goss 1985; Bieging, Goss, & Wilcots 1991; Roberts et al. 1993; Schwarz et al. 1995). Some lines of sight which have also been explored through VLBI and multiepoch pulsar observations have revealed significant opacity variations in the atomic gas on transverse scales down to ~ 10 AU (Dieter, Welch, & Romney 1976; Diamond et al. 1989; Deshpande et al. 1992; Frail et al. 1994; Davis, Diamond, & Goss 1996; Heiles 1997; Faison et al. 1998). The observed opacity variations had raised concerns regarding the origin, lifetime, and pressure equilibrium with the rest of the interstellar medium of the small-scale structure presumed to cause them. Related issues in this context are coherent length scales of the underlying structures, the role of turbulence in producing these, and the power contained in such structures as opposed to that in large-scale structures.

Some of these issues are best addressed through a power spectrum analysis of the H I density fluctuations at the

relevant range of scales. For the warm H I gas observed in emission, this is rather straightforward since the observed 21 cm line intensity is directly proportional to the column density of the H I gas. Thus, the observed line visibilities as a function of spatial frequency define the power spectrum of the H I density fluctuations. For scales of 50–200 pc, this has been carried out by Green (1993), and a useful analytical formulation related to such measurements is discussed by Lazarian (1995). The measurement of H I absorption distribution, on the other hand, cannot be directly interpreted in terms of the power spectrum of the H I density fluctuations, as the H I absorption depends on the integral along the sight line of the ratio of the number density to the spin temperature of the H I gas. Thus, the translation of the observed optical depth fluctuations to those in H I density necessarily involves an assumption about the dependence of the density on temperature (e.g., pressure equilibrium would imply constancy of the product of density and temperature). Direct interpretations of the H I absorption measurements are made difficult by the effects due to the finite extent and the shape of the background source.

More recently, the opacity variations in the cold atomic gas have been imaged using bright supernova remnants as background continuum sources (Bieging, Goss, & Wilcots 1991; Roberts et al. 1993; Schwarz et al. 1995). Some of these observations provide a unique opportunity to study the opacity distributions over a large range of spatial scales. In this paper, we attempt to derive an underlying power spectrum from the H I opacity distribution observed in the direction of two bright radio sources, Cas A and Cygnus A. The power spectrum of the opacity distribution over about 2 orders of magnitude in spatial scales (as from the Cas A data) is found to follow a power law. The optical depth images used in the current analysis are discussed in § 2. The power spectrum analysis and application of CLEAN for high dynamic range spectral estimation are discussed in § 3.

This CLEAN procedure, to recover the true spectrum from the observed spectrum, takes into account the extent and shape of the background source. In § 4, the estimated power spectra of the cold H I gas in the Galaxy toward Cas A are presented. In this section, we also present the structure function of the observed optical depth distribution in the Galaxy toward the direction of both sources. The possible relation between the opacity spectrum and the underlying spectrum of H I density fluctuations is examined in § 4.1. The implications of the derived power spectra of the cold gas for the interstellar medium are discussed in § 5.

2. OPTICAL DEPTH IMAGES

The distribution of cold H I gas in the Galaxy toward the supernova remnant Cassiopeia A ($l \sim 111^\circ$, $b \sim -2^\circ$) was observed by Bieging et al. (1991, hereafter BGW) using the Very Large Array (VLA) of the National Radio Astronomy Observatory. They present optical depth images at an angular resolution of $7''$ and a spectral resolution of 0.6 km s^{-1} . Cas A is at a distance of $\sim 3 \text{ kpc}$ from the Sun and is believed to be in, or beyond, the Perseus spiral arm. The

optical depth image cube presented by BGW covers a velocity range from ~ -30 to -56 km s^{-1} (V_{LSR}). The H I absorption in this velocity range is caused by the interstellar gas in the Perseus spiral arm. An optical depth image in one of the velocity channels (at $V_{\text{LSR}} = -38.8 \text{ km s}^{-1}$) from this cube is reproduced in Figure 1. The morphology of the absorbing gas at an adopted distance of $\sim 2 \text{ kpc}$ to the Perseus arm (spatial resolution $\sim 0.07 \text{ pc}$) is dominated by filaments, loops, and arcs.

Recently, we used the VLA to observe the distribution of cold gas in the Galaxy toward the direction of the powerful extragalactic radio source Cygnus A ($l \sim 75^\circ$, $b \sim 5^\circ$). The observations were carried out with the VLA in the B configuration (maximum baseline $\sim 11 \text{ km}$) on 1999 December 26 and 27. A bandwidth of 1.56 MHz was used with 256 channels and Hanning smoothing, resulting in a spectral resolution of 1.29 km s^{-1} . The synthesized beam was $3''.8 \times 3''.6$ at a position angle of $-2^\circ.8$. Bandpass calibration was achieved by frequency switching on Cygnus A. The channels from the flat portion of the spectrum and free from line absorption were used to estimate continuum visibilities.

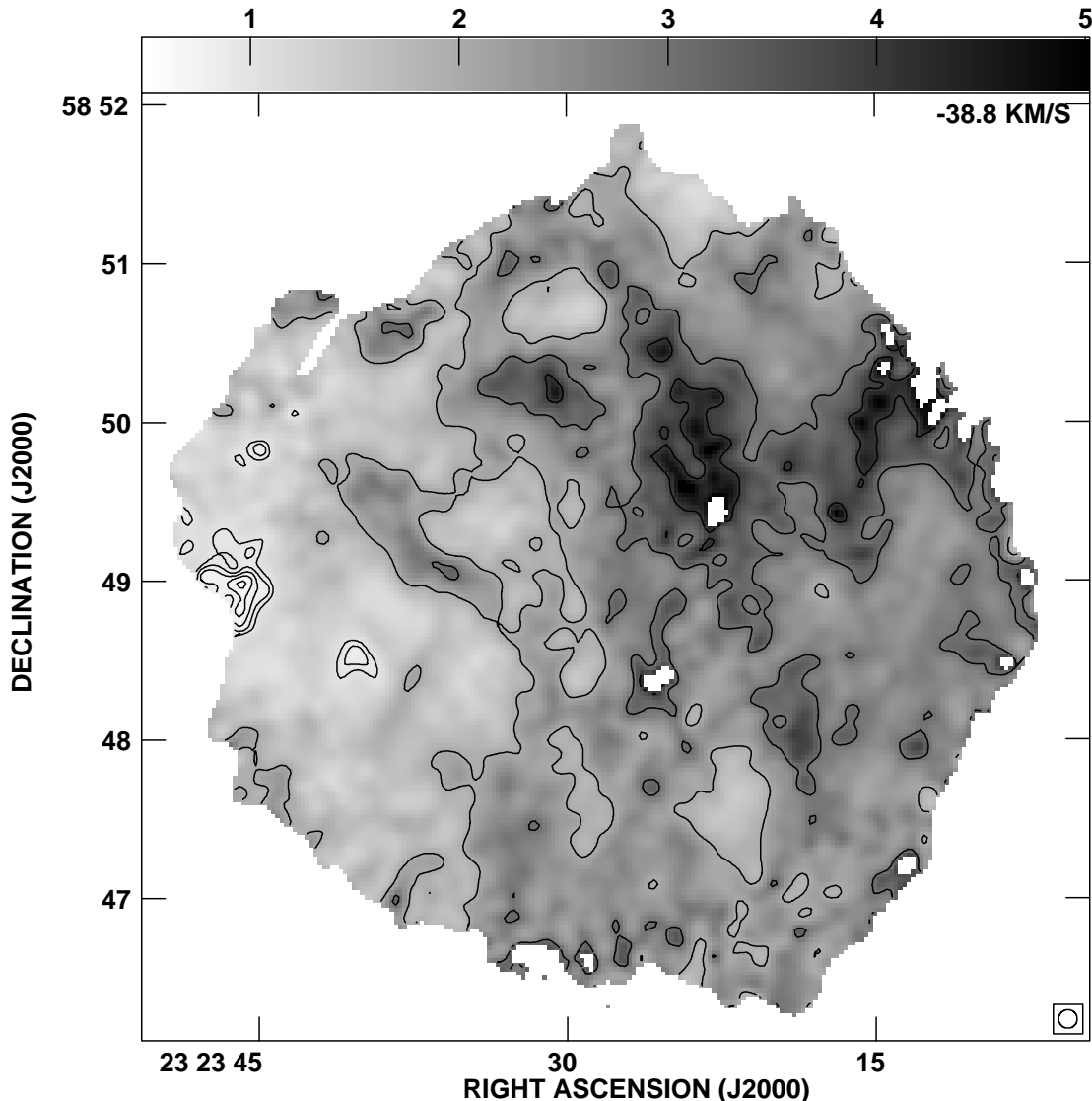


FIG. 1.—H I optical depth image at a $V_{\text{LSR}} = -38.8 \text{ km s}^{-1}$ toward Cas A from BGW. This VLA image has an angular resolution of $7''$ with a sampling interval of $1''.6$. The optical depth gray scale ranges from 0.5 (white) to 5 (black). The contours are in units of 0.1 from 0.1 to 1, and in units of 1 from 1 to 5 in optical depth. The synthesized beam is shown in the bottom right-hand corner. The velocity resolution of this image is 0.6 km s^{-1} .

Spectral line visibilities in each of the relevant spectral channels were obtained by removing the estimated continuum contribution to the visibilities. The images constituting a spectral image cube, as well as the continuum image, were constructed and CLEANed. The rms noise in each of the spectral channels and in the continuum image was 0.1 Jy beam^{-1} , limited by dynamic range. The optical depths (τ) were estimated in the standard way at all positions where

the line intensity and the continuum intensity were greater than 5 times the rms value in the respective images. Some examples of optical depth images produced this way are shown in Figures 2 and 3. The double-lobed morphology is simply a reflection of the radio continuum morphology of Cygnus A. The optical depth images in Figures 2 and 3 provide examples of the distribution of cold atomic gas in the Local and the outer spiral arms, respectively. The

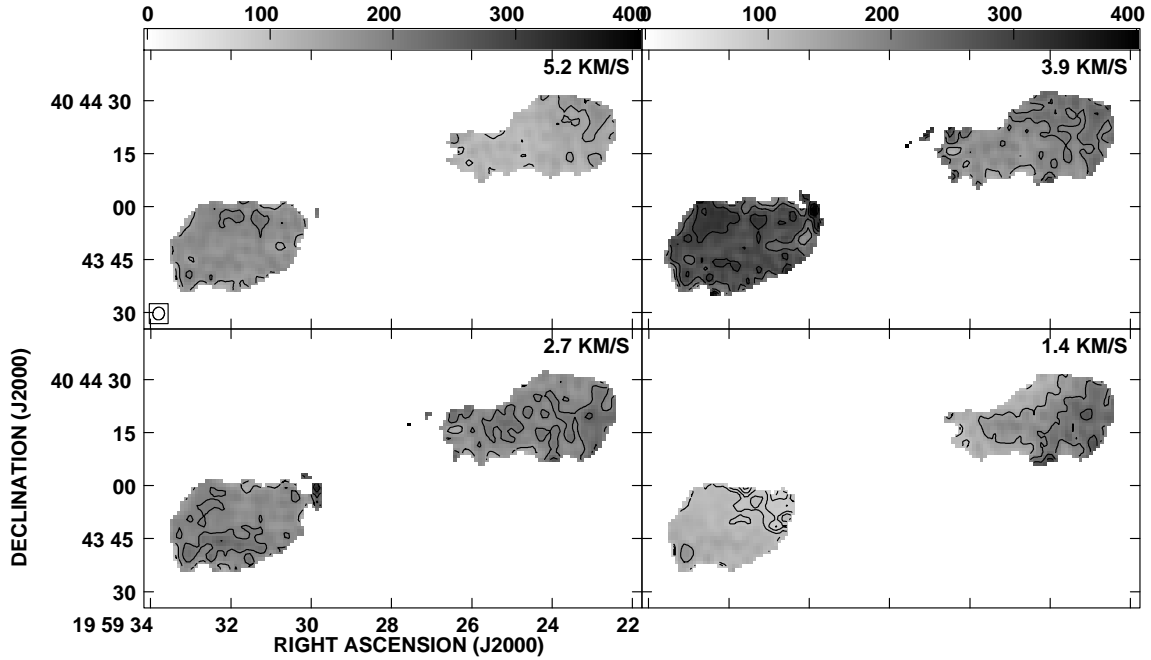


FIG. 2.—H I optical depth image of the Local arm toward Cygnus A produced from the VLA observations described in this paper. The top right-hand corner indicates the V_{LSR} . The bottom left-hand corner of the first panel shows the synthesized beam. The optical depth gray scale ranges from 0 (white) to 0.4 (black). The contours are in units of 0.01 from 0.01 to 0.1, and in units of 0.05 from 0.1 to 0.5 in optical depth. The angular resolution of $\sim 3''.7$ corresponds to a linear resolution $\sim 0.01 \text{ pc}$ for an assumed distance of 0.5 kpc to the Local arm. The sampling interval in these images is $1''$, and the velocity resolution is 1.29 km s^{-1} .

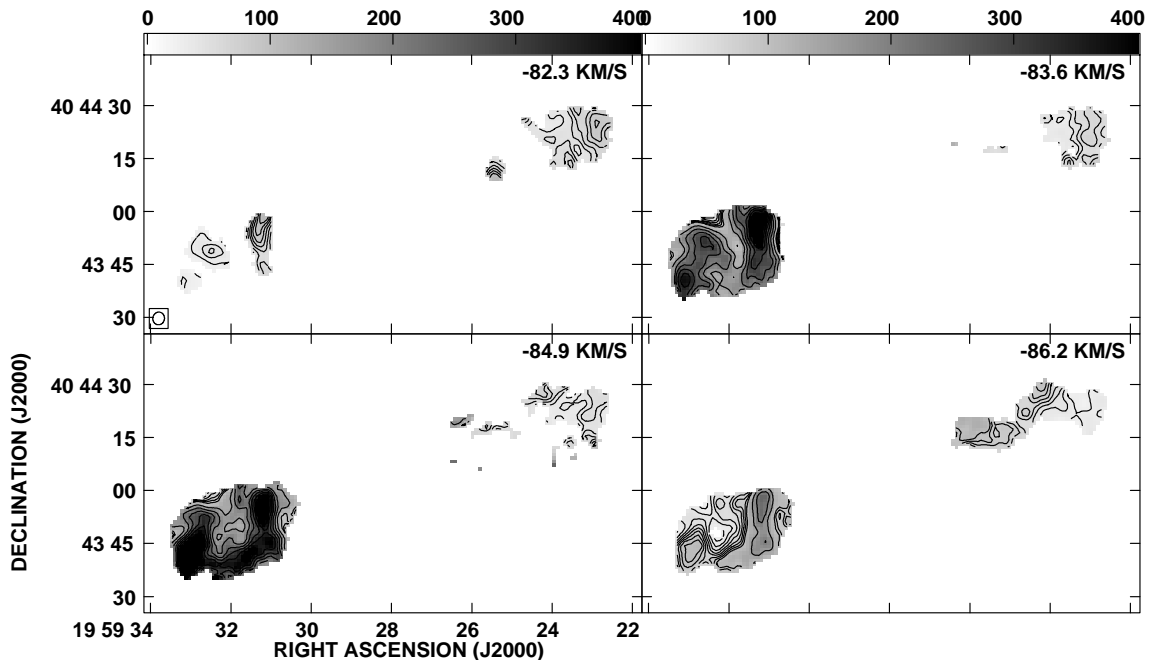


FIG. 3.—H I optical depth image of the outer arm toward Cygnus A obtained from the VLA. The contours are as in Fig. 2. The angular resolution of $\sim 3''.7$ corresponds to a linear size $\sim 0.27 \text{ pc}$ for an assumed distance of 15 kpc to the outer arm.

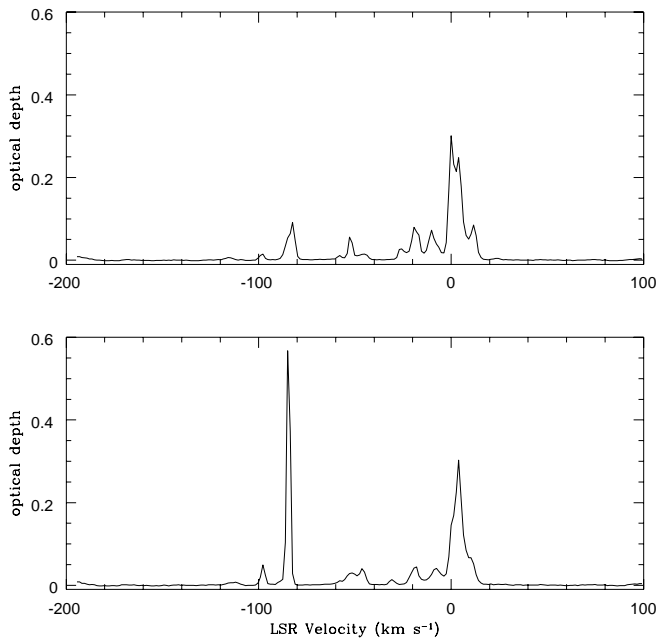


FIG. 4.—Upper and lower frames show the H I optical depth spectra toward the northwest and the southeast peaks of Cygnus A, respectively. Note the large optical depth values corresponding to the Local ($V_{\text{LSR}} 0 \text{ km s}^{-1}$), and the outer ($V_{\text{LSR}} -85 \text{ km s}^{-1}$) arms. In contrast, the Perseus arm shows a weak H I absorption ($\tau < 0.05$) at $V_{\text{LSR}} -50 \text{ km s}^{-1}$.

spatial resolutions of these images correspond to $\sim 0.01 \text{ pc}$ and 0.3 pc at the Local and the outer arms, respectively. The assumed distances to the Local and the outer arms are 0.5, and 15 kpc, respectively. There is very little H I absorption (peak optical depth < 0.05) in the Perseus arm toward Cygnus A (Fig. 4). Consequently, except toward the two brightest positions in the two lobes of Cygnus A, the optical depth of the Perseus arm remains unmeasured toward most of the area covered by the two lobes. These images are not displayed. For the same reason, we also do not use the Perseus arm optical depth images toward Cygnus A in the structure function analysis discussed in § 4.

3. POWER SPECTRUM ANALYSIS

For the first time, the optical depth images in the Cas A direction provide possibilities of studying the distribution of cold H I over a usefully wide range of spatial scales simultaneously. Given the extent and the resolution of these images, a detailed estimate of the power spectrum of the opacity distribution over nearly two decades in spatial scales is possible. In this section, we attempt such an estimate and present details of our analysis.

In an ideal situation, where a fully sampled opacity distribution is available over an extent of θ_{max} and with a sampling interval $\Delta\theta$, it is possible to simply Fourier transform the distribution and estimate the power spectrum over a frequency range $1/\theta_{\text{max}}$ to $1/(2\Delta\theta)$. In reality, the opacity distribution is not fully sampled (see Fig. 1), making it difficult to estimate the true power spectrum directly. As is clear from the distribution in Figure 1, the incomplete sampling is primarily due to the finite extent of the background source, Cas A. In principle, a smaller section of the image where sampling is complete can be chosen; however, reduced resolution in the spectrum then results. Unfortunately, some incompleteness exists in most of the optical

depth images within the source extent where the continuum background or the line intensity is too weak to allow a reliable estimation of the optical depth. If the optical depth at the unsampled locations in the image is assigned zero value, the Fourier transform of the image gives a spectrum that is a convolution of the true spectrum with the Fourier transform of the measurement mask or the *sampling spectrum*. The measurement mask is defined by ones and zeros at the locations that are sampled and unsampled, respectively. This convolution can significantly modify the spectrum, thus making the nature of the true spectrum less apparent. Some form of deconvolution operation is therefore required to recover the true spectrum, particularly when high dynamic range estimation is a primary consideration (as would be while studying steep power-law spectra).

3.1. Application of CLEAN for High-Dynamic-Range Spectral Estimation

The situation in obtaining the true spectrum from the modified or *dirty* spectrum is analogous to that of obtaining a clean image from a dirty image routinely encountered in synthesis imaging (Ryle & Hewish 1960). There, the dirty image obtained from a telescope is the convolution of the clean image with the point spread function (PSF) of the telescope, and the dirty image needs to be deconvolved with the PSF in order to obtain the true (or clean) image. The deconvolution attains even more importance when the telescope is an unfilled aperture. In such a situation, a technique called CLEAN (Högbom 1974) is commonly used to obtain high dynamic range images. In the present situation, the dirty spectrum is to be deconvolved using the spectrum of the mask in order to obtain the true spectrum. The application of CLEAN in the power spectral analysis of nonuniformly sampled pulsar timing data was developed by Deshpande, Allesandro, & McCulloch (1996). In that case, a one-dimensional CLEAN was developed. In the present context, a two-dimensional variant of this application is used. Details of the application of CLEAN in the context of power spectral analysis can be obtained from Deshpande et al. (1996). Only a brief summary of the procedure used in the present context will be given here.

The two-dimensional τ image (e.g., Fig. 1), which is 223×223 pixels, is padded with zeros to obtain a 512×512 image. A mask of the same dimensions is also prepared. This padding helps in improving the sampling by a factor of ~ 2 in the spectral domain, which improves the performance of CLEAN qualitatively, although at the expense of additional computation. Both the image and the mask in the image domain are Fourier transformed to obtain the image spectrum and the mask spectrum in the spatial frequency domain, respectively. The spectra so obtained are Hermitian symmetric (as are visibilities and unlike the images in the case of synthesis imaging), and the CLEAN algorithm was modified to account for this modification: (1) During each iteration of CLEAN, while searching for the maximum in the spectrum, only the amplitudes were considered. But, while removing CLEAN components, the complex nature (amplitude and phase) is taken into account, and (2) the search for the maximum was made only over one-half of the image spectrum. Subsequently, subtraction of a scaled version of the mask spectrum was performed over both halves of the image spectrum after accounting for the Hermitian-symmetric contribution. This procedure ensures the Hermitian symmetry in the CLEAN

spectrum. The CLEAN complex components are restored with a half-cycle cosine of half-power width close to the original spectral resolution which is added to the residuals. The square of the amplitude of the resultant CLEAN complex spectrum is then used to estimate the power spectrum. Finally, an azimuthally averaged one-dimensional power spectrum is obtained from such a two-dimensional CLEAN power spectrum to improve the spectral definition; of course any information on anisotropy is lost. This procedure was applied to a series of optical depth images corresponding to individual velocity channels as well as those integrated over wider velocity ranges. Given the continuous nature of the spectra, one may legitimately question the applicability of the CLEAN deconvolution procedure (Schwarz 1978), since CLEAN assumes a generally empty domain with only well-separated narrow spectral components in the true spectrum. Interestingly, the often encountered steep power-law spectra (power $\propto q^{-\alpha}$, where q is the spatial frequency) are red in nature; i.e., α is positive. When viewed on a linear scale, such spectra would be highly peaked around zero frequency and relatively empty elsewhere, providing a favorable situation for CLEAN.

The azimuthally averaged mask spectrum corresponding to the image in Figure 1 is a featureless power law (power $\propto q^{-\alpha}$, where q is the spatial frequency) with a slope (or power-law index) of 2.9 ($=\alpha$). This spectrum can be understood by noting that the optical depth image in Figure 1 defines an approximately circular area (the morphology of the background source Cas A) as the sampled distribution. The Fourier transform of a uniformly weighted perfect circular patch is an Airy pattern, i.e., a Bessel function of I order divided by q . For large values of its argument (q), the square of the Airy pattern decreases as q^{-3} . Hence, the observed power-law slope of the mask spectrum is not surprising. As an example of the improvement brought about by the CLEAN procedure, Figure 5 shows the azimuthally averaged versions of the dirty spectrum (i.e., pre-CLEAN, *dashed line*) and the clean spectrum (i.e., CLEANed and restored, *solid line*) for the images similar to that in Figure 1. In both cases the power spectra from 11 channels in the velocity range -41.4 to -34.9 km s $^{-1}$ were averaged to improve the spectral definition, since the individual noisy spectra are similar. There are two distinct differences between the two spectra. First, the true spectrum has a knee at $\log(q/q_{\max}) \sim -0.5$ corresponding to the size of the synthesized beam $\sim 7''$. The power spectrum drops sharply beyond these frequencies. This bowl is filled in by the leakage of power from lower frequencies in the dirty spectrum. Second, the slope of the true spectrum is 2.75 while that of the dirty spectrum is 2.4 [both the slopes calculated between -0.5 and -1.5 in $\log(q/q_{\max})$]. The dirty spectrum is expected to be flatter than the CLEAN spectrum since the latter has been convolved with the mask spectrum leading to a mixing (spread) of power from smaller to larger spatial frequencies.

It may be noted that although the processing described so far involves two-dimensional images/spectra, the results are presented as azimuthally averaged versions. This averaging improves the definition of the spectra in a monotonically increasing fashion toward higher spatial frequencies consistent with the increasing number of independent samples available for the averaging. Thus, the uncertainties are relatively high toward the lower spatial frequency end of the spectrum, which is therefore excluded

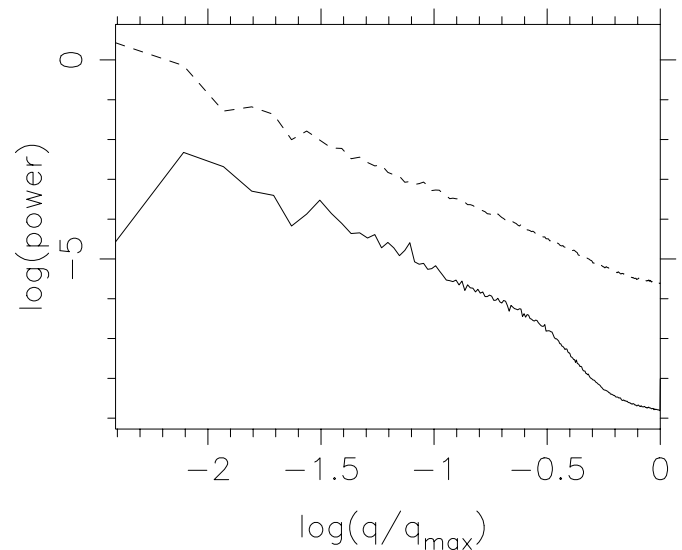


FIG. 5.—Demonstration of the CLEAN procedure in power spectra. The x-ordinate is logarithm of the spatial frequency in units of the limiting frequency (q_{\max}). The limiting frequency is half of the sampling frequency. The sampling interval in the Cas A optical depth images used here is $1''$. The top curve (*dashed line*) is a dirty power spectrum obtained after averaging the power spectra of 11 channels in the velocity range $V_{\text{LSR}} = -41.4$ km s $^{-1}$ to -34.9 km s $^{-1}$. The bottom curve (*solid line*) is the true power spectrum obtained after CLEANing. Note the appearance of the “knee” in this spectrum at $\log(q/q_{\max}) \sim -0.5$. This effect is due to the finite size ($7''$) of the synthesized beam. The slopes of the dirty and true spectra are 2.4 and 2.75, respectively, estimated over the x-range -0.5 to -1.5 .

from any quantitative estimation (e.g., slope). At the other end, the shape of the bowl is a result of the steepening of the spectrum due to beam smoothing and a flattening of the spectrum as the contribution due to the uncertainties in the estimation of optical depth becomes significant. Consideration of these two effects defines the range of spatial frequencies over which the spectral characteristics can be estimated reliably. The CLEAN spectrum viewed over this range is describable by a simple power law of the form $q^{-\alpha}$, where q is the spatial frequency and α is the power-law index.

4. POWER SPECTRA FROM CAS A AND CYGNUS A

The spatial power spectra of optical depth distribution toward Cas A are shown in Figure 6. These spectra represent average description over the velocity intervals -51.6 to -45.2 km s $^{-1}$ and -41.4 to -34.9 km s $^{-1}$ separately. These velocity ranges correspond to the Perseus arm and arise from a distance of 2 kpc. In Figure 6 there are three spectra, obtained as follows:

1. *Case A.*—A power spectrum is obtained for each of the 11 velocity channels in the chosen velocity range (e.g., -51.6 to -45.2 km s $^{-1}$). The resultant 11 power spectra were found to be similar in slope and differing in the spectral density consistent with the optical depth variations in the images used. They were combined with uniform weighting, giving an average description of opacity distribution viewed over a narrow channel (width 0.6 km s $^{-1}$ in the present case). In Figure 6 there are two spectra obtained in this fashion corresponding to the two velocity ranges -51.6 to -45.2 km s $^{-1}$ (*dot-dashed line*) and -41.4 to -34.9 km s $^{-1}$ (*solid line*). These two spectra are less noisy (owing to the averaging over 11 channels) and follow each other well

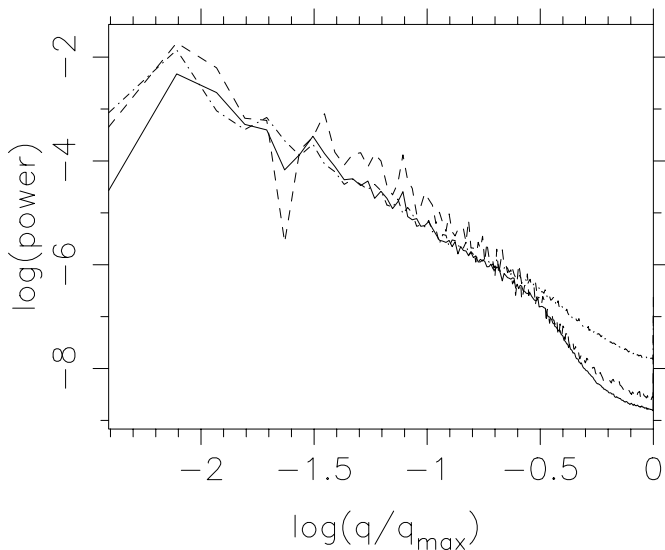


FIG. 6.—Spatial power spectra of optical depth distribution toward Cas A. The spectrum indicated by the solid line is obtained as in case A (§ 4) and corresponds to the velocity range -41.4 to -34.9 km s $^{-1}$. The spectrum indicated by the dot-dashed line also corresponds to case A, but to the velocity range -51.6 to -45.2 km s $^{-1}$. The third spectrum (*dashed line*) is obtained as in case B (see § 4) and corresponds to the velocity range -41.4 to -34.9 km s $^{-1}$. All the three spectra have a slope of 2.75 ± 0.25 (3σ error) over the $\log(q/q_{\max})$ range of -0.5 to -1.5 . However, the case B spectrum has 3 times higher power than the case A spectrum over this range of $\log(q/q_{\max})$.

in the $\log(q/q_{\max})$ range of -1.5 to -0.5 . It is not surprising that the agreement of the power spectra in these two velocity ranges is excellent given the same range of spatial scales covered.

2. *Case B.*—The optical depth images over 11 velocity channels of a chosen velocity range (-41.4 to -34.9 km s $^{-1}$) were first averaged to obtain one image for which a power spectrum was estimated. A given pixel in the average image was blanked when the average could not be performed over all the 11 velocity channels (i.e., when one or more of the channel images had the corresponding pixel blanked). This reduces, however, the total number of valid pixels in the resultant image. This effect was minimized for the velocity range -41.4 to -34.9 km s $^{-1}$. This spectrum is shown in Figure 6 as a dashed line and is easily recognized as the noisiest of the three spectra shown. The slopes estimated over the $\log(q/q_{\max})$ range of -0.5 and -1.5 for all the three spectra are equal within the noise, with a power-law slope of 2.75 ± 0.25 (3σ error). The average power in the case B spectrum (*dashed line*) over this range in $\log(q/q_{\max})$ is about a factor of 3 higher than the two case A spectra. The implications of this enhanced power will be discussed in § 5.

A similar analysis was also attempted for the data in the direction of Cygnus A. However, given the very limited sampling in this case, a structure function should provide a more useful description of the opacity distribution than an azimuthally averaged spectrum, even after CLEANing. Hence, we have obtained the structure function for the observed optical depth distribution toward Cygnus A and compared this with the Cas A results. The structure function of the optical depth is defined as $D_{\tau}(r) = \langle [\tau(x) - \tau(x-r)]^2 \rangle$, where $\tau(x)$ is the optical depth at point x , and the estimation is based on only those points in the image

where the optical depth estimates are considered to be reliable. It can be shown that for a distribution having a power-law spectrum ($\propto q^{-\alpha}$), the structure function will also be a power law ($\propto r^{2\beta}$, where $r \propto 1/q$), such that $\alpha = 2 + 2\beta$ (Lee & Jokipii 1975).

In Figure 7, the square root of the structure function (i.e., the rms fluctuation) of the optical depth distribution in the Perseus arm toward Cas A (*crosses*) is compared with those in the Local (*circles*) and outer arms (*squares*) toward Cygnus A. The spatial scales indicated are appropriate to the assumed distances of the absorbing H I gas. The effect of the beam smoothing is apparent toward the smaller spatial scales (over about half an order of magnitude) in each of the structure functions. Toward the larger spatial scales, the estimation suffers from an inherent limitation in having a limited number of independent realizations of the large-scale variations that are required to obtain a true average estimate. The gap seen in the structure function corresponding to the outer arm of Cygnus A results from inadequate statistics consistent with the absence of optical depth estimates over a large fraction of the northwest lobe (see Fig. 3). Even with these limitations, the reliably estimated sections of the structure functions indicate that the slopes of two of the three determinations (the Perseus arm and the outer arm) are consistent ($\beta \sim 0.4$). In addition, this value of β is consistent with the power law index ($\alpha = 2.75$) for the gas in the Perseus arm (Fig. 6). The slope in the case of the Local arm is significantly shallower ($\beta \sim 0.25$). In addition, the fluctuations in the opacity (and its mean value) are an order of magnitude higher for the gas associated with the Perseus arm of Cas A, as compared to the outer arm H I in the direction of Cygnus A. The vertical heights from the Galactic plane of the H I gas observed in these two cases are different, namely, ~ 70 pc for the gas in the Perseus arm toward Cas A and ~ 1300 pc for the gas in the outer arm toward Cygnus A. However, it is unclear how much of the

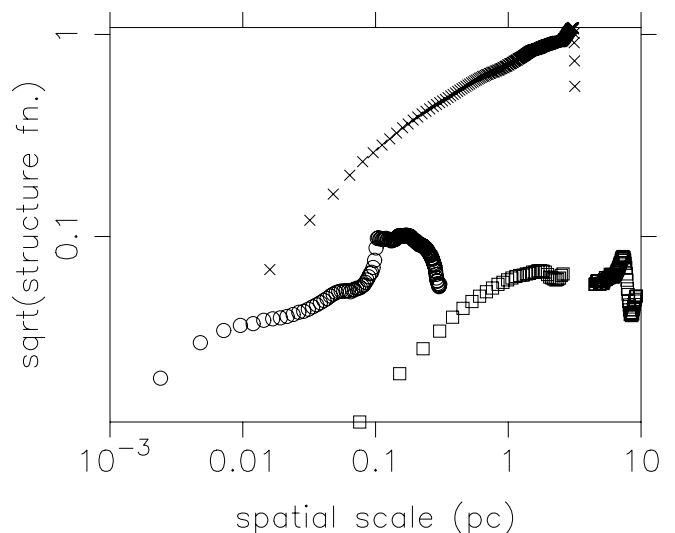


FIG. 7.—Structure function toward Cas A and Cygnus A. The square root of the structure function (i.e., the rms value) of the optical depth distribution in the Perseus arm toward Cas A (*crosses*) is compared with those toward Cygnus A in the Local (*circles*) and the outer (*squares*) arms. The spatial scales correspond to the assumed distances of 0.5, 2, and 15 kpc for the Local, the Perseus, and the outer arms, respectively. See § 4 for further details.

differences seen in the structure functions corresponding to these arms are attributable to the differences in the heights from the Galactic plane of the absorbing H I gas in these two arms.

4.1. Implications for the Distribution of H I Density and for Pressure Equilibrium

The derived (CLEAN) power spectra shown in Figure 6 represent $p_i(k)$, the spatial power spectrum of the optical depth distribution. The optical depth, τ , is related to the column density (N_H) and (density weighted harmonic) mean spin temperature (T_s) of the H I gas as $\tau \propto N_H/T_s$. The column density of H I is related to the volume density (n_H) as $N_H = n_H l$, where l is the line of sight path length of the H I gas. The pressure of the H I gas (P) viewed locally is related to the volume density and kinetic temperature (T_k) as $P \propto n_H T_k$, assuming it to be a perfect gas. For the cold gas in the Galaxy, $T_s \approx T_k$. If the different density regions are in pressure equilibrium (i.e., $n_H \propto 1/T_k$) with each other, then this implies that $\tau \propto n_H^2$. In general, if the equation of state for the cold H I gas is given by $T_k \propto n_H^\gamma$, then the optical depth will be proportional to $n_H^{1-\gamma}$. Pressure equilibrium corresponds to $\gamma = -1$. It is not straightforward to predict the power-law index of the density spectrum based on that of the observed optical depth. However, it is possible to explore the relation between these two through suitable Monte Carlo simulations involving an assumed power-law spectrum of density and a value of γ . Our attempts to do so have indicated that the slope of the computed power spectrum of opacity is nearly the same as that of the assumed slope of the three-dimensional power spectrum for the H I density. The two slopes differ marginally if, in the assumed density distribution, the density fluctuations far exceeded the mean density. Otherwise, the resultant slope showed no dependence on the assumed value of γ , indicating that the assumption of pressure equilibrium is reasonable. This independence of the slope on the assumed value of γ is not surprising since any nonlinear dependence of τ on n_H implied by the equation of state ($\tau \propto n_H^{1-\gamma}$) reduces to the first order to a dominant linear dependence [$\delta\tau \propto (1-\gamma)\delta n_H$] if the fluctuation in density (δn_H) is small compared to the mean density ($\langle n_H \rangle$). Hence, the nature of the observed spectrum of τ distribution must closely describe the corresponding spectrum of the H I density.

5. DISCUSSION

As can be seen in Figure 6, the spectrum obtained in case B (spectrum of the optical depth averaged over several velocity channels) has about a factor of 3 higher power than the case A spectrum (average of the spectra of several velocity channels). This difference indicates that there is partial correlation in structures as a function of velocity. The spectra are normalized suitably, such that if the structures were fully correlated across N channels, we would observe an increase in power by a factor of N . Hence, the observed increase by a factor of 3 in power indicates a correlation scale of $\sim 2 \text{ km s}^{-1}$ in velocity. This correlation scale in velocity is expected since the typical value of turbulence for the cold H I gas in the Galaxy is $\sim 4 \text{ km s}^{-1}$ (Radhakrishnan et al. 1972).

The power spectrum of density fluctuations in the cold atomic gas toward Cas A has a slope of ~ 2.75 . Adopting a distance of 2 kpc for this absorbing gas, the linear scales probed ranged between 0.07 and 3 pc, corresponding to the

resolution ($7''$) and the size of Cas A ($\sim 5'$), respectively. Compared to these transverse scales, the longitudinal (or the line of sight) scales corresponding to each of the channels (i.e., velocity resolution) must be significantly larger. Otherwise, the power spectrum obtained from the integrated image (case B) should have a different (steeper) slope compared to that for a single-channel image (case A). However, as has been demonstrated in Figure 6, there is no significant difference in the two slopes. Thus, the opacity image in a single channel corresponds to a longitudinally integrated version of the underlying three-dimensional opacity distribution. Combining this result with the discussion in § 4, the power spectrum represents the three-dimensional power spectrum of density fluctuations in the cold atomic gas over linear scales of 0.07–3 pc. The H I emission analysis (Green 1993) provided a similar slope over the larger scales of 50–200 pc. Assuming no changes in the slope of the power spectrum between these two ranges, a constant slope is implied over 3 orders of magnitude in linear scales. It is noteworthy that the estimated slope of 2.75 for the power spectrum differs significantly from the Kolmogorov slope ($11/3 = 3.67$) expected for the three-dimensional power spectrum of a turbulence-dominated incompressible fluid.

In a recent paper, Lazarian & Pogosyan (2000) draw attention to the modification of the H I density spectrum due to the velocity field. They point out that the velocity range needs to be thick in order to obtain the true density power spectrum. They estimate a power-law index close to the Kolmogorov value for the power spectrum of density using the H I emission data of the Galaxy (Green 1993) and of the Small Magellanic Cloud (Stanimirovic et al. 1999). Being aware of this complication, we have obtained the power spectra before (case A) and after (case B) averaging in velocity (§ 4). Within the errors of estimation, the two slopes agree (Fig. 6), indicating that the effect of averaging over velocity is not a substantial effect.

It may not be surprising that the slope of the power spectrum of density fluctuations in the cold atomic gas in the Galaxy is different from the Kolmogorov slope considering that (a) the H I gas in the interstellar medium is compressible, and (b) the Kolmogorov index is expected if the energy input into the interstellar medium at some large scale cascades down to small scales through a turbulence mechanism. However, the exact nature and the scales at which the energy is input and its cascade to smaller scales are determined by a range of processes in the interstellar medium such as the supernovae and stellar winds. Although a qualitative discussion of many such aspects is available (Lazarian 1995), the quantitative implications of these processes on the slope of the power spectrum is quite uncertain.

Another important implication of the derived power spectral description is to the long-standing puzzle of the observed opacity variations on small transverse scales down to tens of AU. These opacity variations have been interpreted in the past as evidence for widespread small-scale structure in the H I distribution, with volume densities orders of magnitude higher than those implied by the parsec-scale component. It has been recently emphasized (Deshpande 2000) that there is a need to recognize the nature of the actual quantity measured at small scales; almost all scales contribute to the measured opacity differences at small scales. Furthermore, if the power spectrum with a slope of 2.75 estimated for the Cas A Perseus arm

data is extrapolated to these small scales, optical depth variations with an rms of 0.1 can be expected on scales of ~ 100 AU (Deshpande 2000). The recent H I absorption measurements using the Very Long Baseline Array and the Very Large Array indicate that five out of the seven sources observed show opacity variations consistent with this extrapolation (Faison et al. 1998; Faison & Goss 2000). However, 3C 138 and 3C 147 show optical depth fluctuations an order of magnitude larger over linear sizes of 10–20 AU indicating real two-dimensional structures in H I opacity, but note that the associated spectra appear much shallower than in the Cas A case.

Our investigations in two different directions (Cas A and Cygnus A) have shown both similarities and differences in

the derived descriptions in terms of slopes and powers associated with the power spectra (and structure functions) of the H I distribution. For a relatively complete picture to emerge, it is desirable that such studies are carried out in different directions in the Galaxy.

The analysis software used here was based largely on a package developed by J. Rajagopal with one of us (A.A.D.). We would like to thank R. Nityananda and V. Radhakrishnan for useful discussions and comments on the manuscript. National Radio Astronomy Observatory is a facility of the National Science Foundation operated under cooperative agreement by Associated Universities, Inc.

REFERENCES

- Bieging, J. H., Goss, W. M., & Wilcots, E. M. 1991, *ApJS*, 75, 999
 Bregman, J. D., Troland, T. H., Forster, J. R., Schwarz, U. J., Goss W. M., & Heiles, C. 1983, *A&A*, 118, 157
 Clark, B. G. 1965, *ApJ*, 142, 1398
 Clark, B. G., Radhakrishnan, V., & Wilson, R. W. 1962, *ApJ*, 135, 151
 Crovisier, J., Dickey, J. M., & Kazes, I. 1985, *A&A*, 146, 223
 Davis, R. J., Diamond, P. J., & Goss, W. M. 1996, *MNRAS*, 283, 1105
 Deshpande, A. A. 2000, *MNRAS*, 317, 199
 Deshpande, A. A., Alessandro, F. D., & McCulloch, P. M. 1996, *J. Astrophys. Astron.*, 17, 7
 Deshpande, A. A., McCulloch, P. M., Radhakrishnan, V., & Anantharamaiah, K. R. 1992, *MNRAS*, 258, 19
 Diamond, P. J., Goss, W. M., Romney, J. D., Booth, R. S., Kalberla, P. M. W., & Mebold, U. 1989, *ApJ*, 347, 302
 Dieter, N. H., Welch, W. J., & Romney, J. D. 1976, *ApJ*, 206, L113
 Faison, M. D., & Goss, W. M. 2000, *AJ*, submitted
 Faison, M. D., Goss, W. M., Diamond, P. J., & Taylor, G. B. 1998, *AJ*, 116, 2916
 Field, G. B. 1973, *Molecules in the Galactic Environment*, ed. M. G. Gordon & L. E. Snyder (New York: Wiley), 21
 Field, G. B., Goldsmith, D. W., & Habing, H. J. 1969, *ApJ*, 155, L113
 Frail, D. A., Weisberg, J. M., Cordes, J. M., & Mathers, C. 1994, *ApJ*, 436, 144
 Green, D. A. 1993, *MNRAS*, 262, 327
 Greisen, E. W. 1973, *ApJ*, 184, 363
 Heiles, C. 1997, *ApJ*, 481, 193
 Högbom, J. A. 1974, *A&AS*, 15, 417
 Kalberla, P. M. W., Schwarz, U. J., & Goss, W. M. 1985, *A&A*, 144, 27
 Lazarian, A. 1995, *A&A*, 293, 507
 Lazarian, A., & Pogosyan, D. 2000, *ApJ*, 537, 720
 Lee, L. C., & Jokipii, J. R. 1975, *ApJ*, 201, 532
 Lockhart, I. A., & Goss, W. M. 1978, *A&A*, 67, 355
 Radhakrishnan, V., Goss, W. M., Murray, J. D., & Brooks, J. W. 1972, *ApJS*, 24, 49
 Roberts, D. A., Goss, W. M., Kalberla, P. M. W., Herbstmeier, U., & Schwarz, U. J. 1993, *A&A*, 274, 427
 Ryle, M., & Hewish, A. 1960, *MNRAS*, 120, 220
 Schwarz, U. J. 1978, *A&A*, 65, 345
 Schwarz, U. J., Goss, W. M., Kalberla, P. M., & Benaglia, P. 1995, *A&A*, 299, 193
 Schwarz, U. J., Troland, T. H., Albinson, J. S., Bregman, J. D., Goss, W. M., & Heiles, C. 1986, *ApJ*, 301, 320
 Stanimirovic, S., Staveley-Smith, L., Dickey, J. M., Sault, R. J., & Snowden, S. L. 1999, *MNRAS*, 302, 417